



**HAL**  
open science

## Localized modes prediction in a membrane with non-uniform tension from the quasi-static measurement of its localization landscape

Carlos García A, Nicolas Dauchez, Yorick Buot de L'Epine, Gautier Lefebvre

### ► To cite this version:

Carlos García A, Nicolas Dauchez, Yorick Buot de L'Epine, Gautier Lefebvre. Localized modes prediction in a membrane with non-uniform tension from the quasi-static measurement of its localization landscape. *Journal of Sound and Vibration*, 2021, 511, pp.116272. 10.1016/j.jsv.2021.116272. hal-03313166

**HAL Id: hal-03313166**

**<https://hal.science/hal-03313166>**

Submitted on 4 Aug 2021

**HAL** is a multi-disciplinary open access archive for the deposit and dissemination of scientific research documents, whether they are published or not. The documents may come from teaching and research institutions in France or abroad, or from public or private research centers.

L'archive ouverte pluridisciplinaire **HAL**, est destinée au dépôt et à la diffusion de documents scientifiques de niveau recherche, publiés ou non, émanant des établissements d'enseignement et de recherche français ou étrangers, des laboratoires publics ou privés.



Distributed under a Creative Commons Attribution - NonCommercial - NoDerivatives 4.0 International License

# Localized modes prediction in a membrane with non-uniform tension from the quasi-static measurement of its localization landscape.

Carlos García A.<sup>a</sup>, Nicolas Dauchez<sup>a</sup>, Yorick Buot de l'Epine<sup>a</sup> and Gautier Lefebvre<sup>a</sup>

<sup>a</sup>Sorbonne Universités, Université de technologie de Compiègne (UTC), Laboratoire Roberval, FRE CNRS 2012, CS 60319 Compiègne cedex, France

---

## ARTICLE INFO

### Keywords:

Landscape of localization  
Heterogeneous membrane  
Non-uniform tension field  
Quasi-static regime

## ABSTRACT

In this paper, an experimental methodology is presented in order to extract the dynamic properties of localized modes of a complex membrane. By applying the *localization landscape* theory, the resonant frequencies and regions of the localized modes can be obtained experimentally. This is implemented by a quasi-static measurement of the membrane deformation, and is performed without the knowledge of its tension field or any hypothesis about its homogeneity (uniform or non-uniform). The results are compared with Finite Element simulations and modal measurements in vacuum conditions.

---

## 1. Introduction

Localization is a term that may refer to different concepts: the process of identifying the location of a specific measurable quantity, i.e. source localization; or the energy concentration within a system, the main interest of this paper. The latter is achievable by focalizing energy into a point, called focal point. This can be obtained by changing the geometry of reflectors or the properties of the propagation medium, as seen in lenses [1] and parabolic antennas, or by the convergence of one or multiples sources into a zone, as used in lithotripsy [2]. Reversal propagation techniques [3] are other means for energy localization. When dealing with standing waves, localization is used to get high levels for acoustic levitation [4, 5], acoustic tweezers [6] or nonlinear ultrasound demodulation [7].

The present paper deals with localized vibrational modes. Commonly, in a complex structure, when a localized vibration is presented, it can be seen as a local mode, existing only in a small area of the structure, in opposition to a global mode, involving the whole structure. Local modes or more precisely localized modes are a common phenomenon studied in vibrations, for example when performing sub-structuring processes.

As a general physical phenomenon, localized waves have been studied in optics, electromagnetism, acoustics and many physical domains. Strong or Anderson localization [8] and weakly localized waves have special attention in optics and in quantum mechanics, due to the disordered media, but also can be found in mechanical waves. Multiples experiments have been carried out such as [9], where localized states were observed in a complex wire; Even et al. [10] implemented the first experiment with localization in fractal drums, showing the presence of both strong and weak localization; Chulkin et al. [11] revealed the appearance of weak localization and its implications on the damping coefficient in a dielectric chain crystal. More recently, Filoche and Mayboroda [12] exposed that even a simple clamped point in a thin plate can induce strong localization.

The work of Filoche and Mayboroda led to an important discovery: both Anderson and weak localization are representations of the same phenomenon and can be unified by the landscape of localization theory [13]. The landscape of localization exposes the presence of localized regions, where the modes can be present, by splitting the whole structure into several regions determined exclusively by the geometry and the operator which describes the motion (Laplacian, Bi-Laplacian or Hamiltonian operators). Lefebvre et al. [14] showed that one static measurement can provide low-frequency information about the dynamic behaviour of a complex plate: geographical placement of the localized modes, their eigenfrequencies and their localized state given by the network of valley lines.

In the domain of structural vibrations, and mainly in vibroacoustics, plates and shells have been the subject of many works (see books of Fahy and Gardonio [15], Norton and Karczub [16], Lesueur [17], Soedel [18] for instance), while membranes dynamics is commonly first introduced because of its relative simplicity in vacuum conditions [19].

---

ORCID(s):

This is the case when uniform tension and density are considered and this assumption does not hold anymore when a non-uniform tension is presented. Much of the research dealing with membranes is centred on the musical domain [20, 21, 22], although membranes are widely present, from the auditory system [23] to room acoustics [24]. To the knowledge of the authors, complex membranes presenting localized modes have been little studied, except in the case of fractal boundary conditions [10].

The aim of this paper is to show how the landscape of localization theory enables to determine the localized modes in a heterogeneous membrane without knowledge of its tension field. Even if the motion of a membrane with uniform tension is a well-known problem governed by the wave equation, imposing a uniform tension field is an arduous task and cannot always be guaranteed. In this sense, configurations with uniform and non-uniform tension are presented in this work, and a complete methodology for extracting the dynamic properties with one quasi-static measurement using laser vibrometry is exhibited. The paper is organized as follows: first, the theoretical background and the landscape of localization theory applied to a heterogeneous membrane are presented. Then, simulations of the landscape function and modal decomposition are exposed to illustrate the general characteristics of the localization landscape. An experimental method is then established to measure the landscape function in a membrane having localized modes. Finally, the results from the landscape of localization theory are compared with experimental modal analysis made in vacuum conditions.

## 2. Theoretical Background

### 2.1. Membrane dynamics

The tension field on a membrane is characterized by the symmetric tensor  $\boldsymbol{\tau}(\mathbf{r})$ , where  $\tau_{ij}$  are the components of the tensor and  $ij$ , being  $x$  or  $y$  as the tension is in the plane, and respecting a valid tension field [25, 26]. The vertical displacement  $w$  of a heterogeneous membrane with surface density  $\rho_s(\mathbf{r})$  can be derived by taking the small displacements hypothesis, where rotations  $\theta_x, \theta_y$  on the planes  $(x, z)$ ,  $(y, z)$  are approximated as  $\theta_x \approx \partial w / \partial x$  and  $\theta_y \approx \partial w / \partial y$ . Exposing the equilibrium of forces and projecting them onto the  $z$  plane [27] results in

$$\rho_s(\mathbf{r}) \frac{\partial^2 w}{\partial t^2} - \text{div}(\boldsymbol{\tau}(\mathbf{r}) \cdot \mathbf{grad}(w)) = 0. \quad (1)$$

In the case of a homogeneous membrane under uniform tension field, the tension becomes isotropic and the tensor  $\boldsymbol{\tau}(\mathbf{r})$  can be reduced to  $\boldsymbol{\tau} = T \cdot \mathbb{1}$ ,  $\mathbb{1}$  being the identity matrix and  $T$  the uniform tension on the membrane. Taking this into consideration

$$T \text{div}(\mathbf{grad}(w)) = T \nabla^2 w = \rho_s \frac{\partial^2 w}{\partial t^2}, \quad (2)$$

and thus

$$\frac{\partial^2 w}{\partial t^2} - c^2 \nabla^2 w = 0. \quad (3)$$

where  $c = \sqrt{T/\rho_s}$  is the speed of sound in the membrane and  $\nabla^2$  the Laplace operator.

### 2.2. The eigenvalue problem

The displacement can be expressed as an infinite sum of orthogonal basis functions, determined by the eigenvalue problem. In a modal decomposition, this results in mode shapes  $\phi_p$  and associated resonant frequencies  $\omega_p^2$ , where each mode satisfy the dynamic equation (Eq. (1)). Imposing fixed boundary conditions results in the Dirichlet problem

$$\begin{aligned} L\phi_p &= \omega_p^2 \phi_p & \text{in } S, \\ w &= 0 & \text{on } \partial S. \end{aligned} \quad (4)$$

where the spatial operator  $L = -\rho_s(\mathbf{r})^{-1} \nabla \cdot (\boldsymbol{\tau}(\mathbf{r}) \cdot \nabla)$  in the case of a heterogeneous membrane, and which can be simplified as  $L = -c^2 \nabla^2$  for a homogeneous membrane.

### 2.3. Quasi-static limit

When the membrane is subjected to uniform harmonic pressure, Eq. (1) becomes

$$\rho_s(\mathbf{r}) \frac{\partial^2 w}{\partial t^2} - \text{div}(\boldsymbol{\tau}(\mathbf{r}) \cdot \mathbf{grad}(w)) = P \cos(\Omega t). \quad (5)$$

where  $\Omega$  is the excitation frequency and  $P$  the amplitude of the imposed pressure. Expressing the displacement in a modal expansion, the forced response results in

$$w = \sum_p \frac{P}{m_p} \frac{\phi_p}{\omega_p^2 - \Omega^2} \iint_S \phi_p \, dS \cos(\Omega t), \quad (6)$$

The resonant frequency of the  $p$  mode is  $\omega_p^2 = k_p/m_p$ , where  $k_p$  is the modal stiffness and  $m_p$  the modal mass, defined as

$$m_p = \iint_S \rho_s(\mathbf{r}) \phi_p^2 \, dS, \quad (7)$$

$$k_p = \iint_S \phi_p \left( \tau_{xx} \frac{\partial^2 \phi_p}{\partial x^2} + \tau_{yy} \frac{\partial^2 \phi_p}{\partial y^2} + 2\tau_{xy} \frac{\partial^2 \phi_p}{\partial x \partial y} \right) dS.$$

The quasi-static regime is expected when the excitation frequency is small in comparison with the first resonant frequency, that is  $\Omega \ll \omega_0$ . In Eq. (6),  $\Omega$  tend to zero and given that  $m_p \omega_p^2 = k_p$ , the quasi-static regime tends to the static case, where no mass is involved

$$w \sim \sum_p \frac{P}{k_p} \phi_p \iint_S \phi_p \, dS. \quad (8)$$

In practice, when  $\Omega = \omega_0/10$ , the relative error between the quasi-static deformation and the static deformation is below 1%. Hence, ten times below the first resonance, the quasi-static and static deformations can be considered equivalent.

### 2.4. Evaluation of the tension from the static deformation

To estimate the tension of the uniform membrane (see Section 4.4.1), we derive the relation between the tension and the maximum displacement of the membrane under static load. The static problem is derived from Eq. (5) as

$$-\text{div}(\boldsymbol{\tau}(\mathbf{r}) \cdot \mathbf{grad}(w)) = P. \quad (9)$$

Under the assumption of an uniform tension field, the tension becomes independent of the operator, as stated in Eq. (2). By imposing fixed boundary conditions, Eq. (9) becomes a standard Poisson problem

$$\begin{aligned} -T \nabla^2 w &= P & \text{in } S, \\ w &= 0 & \text{on } \partial S. \end{aligned} \quad (10)$$

For a circular membrane, the static displacement is expanded in a sum orthogonal basis functions  $\phi_p$  that also satisfy the eigenvalue problem, and scaled by amplitude coefficients  $\alpha_p$

$$w(r, \theta) = \frac{P}{T} \sum_p \alpha_p \phi_p = \frac{P}{T} \sum_{m=0}^{\infty} \sum_{n=1}^{\infty} \alpha_{mn} J_m(\chi_{mn} r/a) \cos(m\theta), \quad (11)$$

where  $J_m$  is the first order Bessel function,  $\chi_{mn}$  the zeros of  $J_m$ , and  $a$  the membrane's radius. The amplitude coefficients  $\alpha_{mn}$  are calculated as

$$\begin{aligned} \alpha_{0n} &= \frac{2a^2}{(\chi_{0n})^3 J_1(\chi_{0n})}, \\ \alpha_{mn} &= \frac{2}{\pi(\chi_{mn})^2 (J_{m+1}(\chi_{mn}))^2} \int_0^a \int_{-\pi}^{\pi} J_m(\chi_{mn} r/a) \cos(m\theta) r \, dr \, d\theta. \end{aligned} \quad (12)$$

Note that the homogeneous case of Eq. (8) is analogous to Eq. (11). Finally, by taking the maximum displacement  $w_{\max}$  of the membrane at  $r = 0$ , it is possible to note that all  $J_m(r = 0)$  are equals to 0 when  $m \neq 0$  on this point. Taking this into consideration, the tension of the membrane relates directly to the maximal displacement

$$T = \frac{P}{w_{\max}} 2a^2 \sum_{n=1}^{\infty} \frac{1}{(\chi_{0n})^3 J_1(\chi_{0n})}. \quad (13)$$

## 2.5. The landscape of localization theory

As described in [13], the low-frequency behaviour is fully described by the landscape of localization theory, summarized in the Dirichlet problem

$$\begin{aligned} Lu &= 1 & \text{in } S, \\ u &= 0 & \text{on } \partial S. \end{aligned} \quad (14)$$

where  $u$  is the landscape function and  $L$  is the spatial operator previously introduced describing the motion of a membrane. Eqs. (9) and (14) are then equivalent; the static deformation and the landscape function differ only by a constant factor so that

$$u = \frac{\rho_s w}{P}. \quad (15)$$

In practice, this relationship allows to determine the landscape function from the measured static deformation of the membrane, which could, in turn, be approximated by its quasi-static deformation (see Eq. (8)).

The landscape theory is a tool for investigating multiple localized modes in a complex structure. The separation between each localized mode is marked by a network of valley function. The set of these valley lines are the minima of the landscape function, that is the lowest gradient regions, and can be obtained by inverse flooding algorithms like the watershed algorithm [28]. The network of valley lines is frequency-dependent and constrains the local displacement of the eigenmodes. Each eigenmode satisfies the inequality [13]

$$\|\phi_p\| \leq \omega_p^2 u \quad \text{in } S. \quad (16)$$

where  $\phi_p$  is normalized such that the maximum amplitude equals 1. When increasing the frequency, the valley will open, allowing the modes to exist beyond the initial localized state.

Based on the similarity of the landscape with the first localized modes, we can obtain an approximation to the eigenfrequencies of the  $i_{th}$  localized mode in each sub-region  $u_i$  of the landscape [14]

$$\omega_i \approx (4/\pi) / \sqrt{\max(u_i)}. \quad (17)$$

## 3. Simulations

To illustrate the application of the landscape theory to a membrane, a finite element calculation of Eq. (14) is implemented in FreeFem++ [29]. The subject of study is a circular membrane of radius  $a = 0.279$  m (22 inches diameter).

To induce localization, two areas inside the domain will be set up with null displacement conditions. Uniform tension about  $1892 \text{ N.m}^{-1}$  and a non-uniform tension field are tested. For the last case, the tension field is established in order to respect  $\text{div}(\tau) = 0$  [25, 26] and the components  $\tau_{xx}$  and  $\tau_{yy}$  of the tensor  $\tau$  are established as linear functions of  $y$  and  $x$  respectively, giving a tension field varying from  $250 \text{ N.m}^{-1}$  to  $750 \text{ N.m}^{-1}$  in each case. No shear tension was taken into account at this stage.

The results of the landscape simulations are presented in Fig. 1 and the first four modes of the membrane in Fig. 2. The white lines represent the network of valley lines of the landscape function, and superimposing these lines onto the modes, according to Eq. (16), provide insights concerning the strength of the confinement of each mode and will be explained more in detail in the experimental section. These lines follow the lowest gradient points, dividing the structure into 2 sub-regions where modes localize. It is seen that the area of the sub-region of each localized mode depends on the tension field. The red crosses mark the peak values in each of the two sub-regions and the amplitude of these peaks will be used, according to Eq. (17), to estimate the frequencies of the localized modes.

Localized modes prediction in a membrane with non-uniform tension from the quasi-static measurement of its localization landscape.

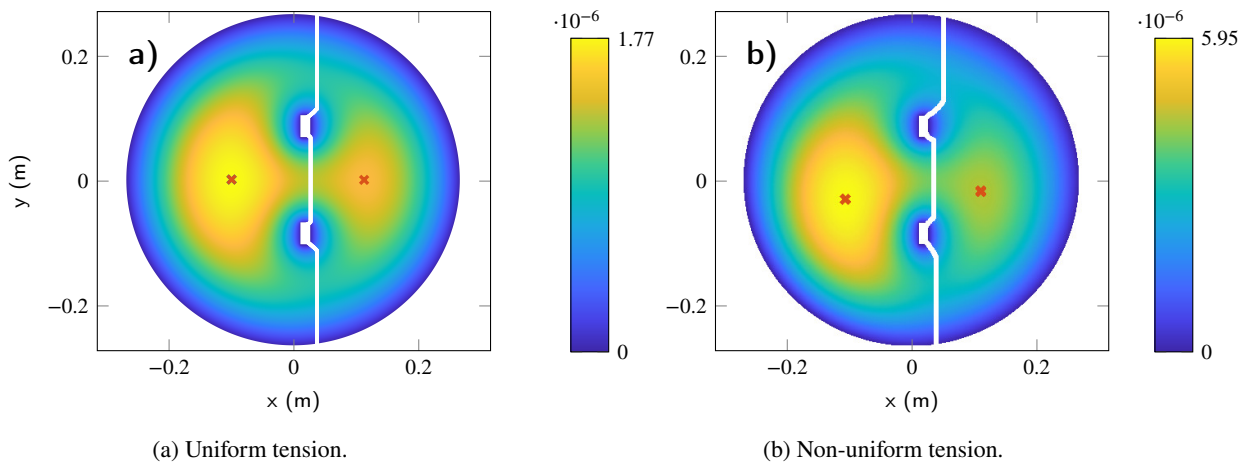


Fig. 1: Landscape simulation,  $u$  ( $s^2$ ).

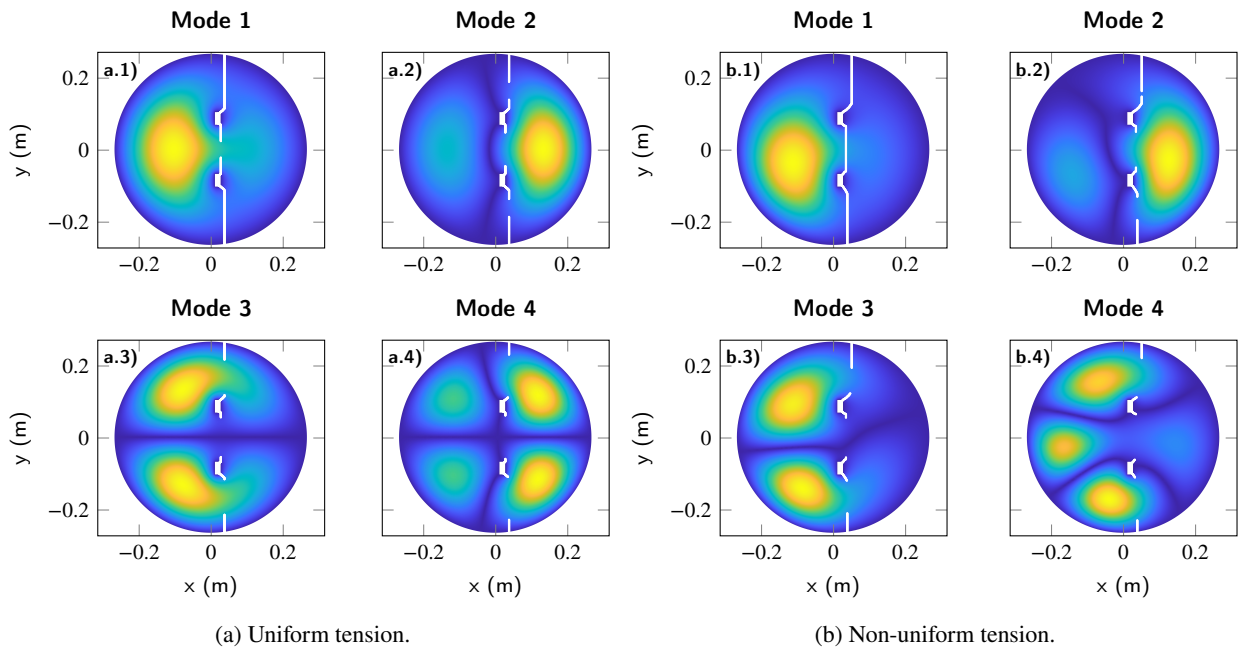


Fig. 2: Mode shape simulation

Table 1

Simulation: Membrane under two different tension fields. [1] Computed with FreeFem++ [2] Calculated with Eq. (17)

	Uniform Tension			Non-uniform Tension		
	FEM <sup>1</sup> (Hz)	Landscape <sup>2</sup> (Hz)	diff. %	FEM <sup>1</sup> (Hz)	Landscape <sup>2</sup> (Hz)	diff. %
<b>Mode 1</b>	144.68	151.49	+4.7	79.66	83.09	+4.30
<b>Mode 2</b>	170.12	166.22	-2.29	99.09	97.98	-1.12
<b>Mode 3</b>	196.55	-	-	107.17	-	-
<b>Mode 4</b>	225.95	-	-	128.72	-	-

Localized modes prediction in a membrane with non-uniform tension from the quasi-static measurement of its localization landscape.

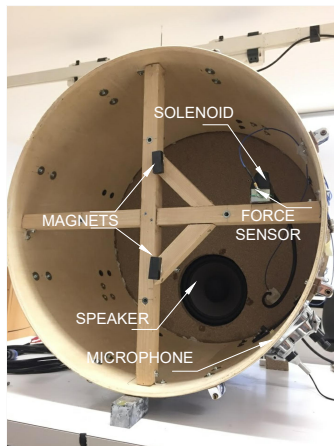
In both cases, it is clear that the two first membrane modes correspond to the two first localized modes in each sub-region. The behaviour changes in the fourth mode, where there is a shift in the appearance of the modes. The resonant frequencies are well predicted by the landscape theory, with a difference of less than 5% (refer to Table 1).

## 4. Experimental Approach

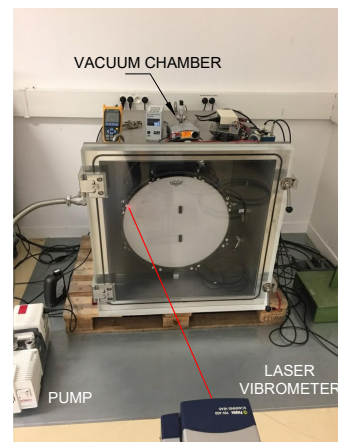
The complete experimental approach is described in four sections: a description of the experimental setup, the modal analysis of the membrane, the landscape function measurement and finally some details about the procedure to set up the membrane's tension.

### 4.1. General configuration

The experimental setup is depicted in Fig. 3. A 22-inch mylar membrane, with density  $\rho = 1380 \text{ kg.m}^{-3}$  and thickness  $e = 254 \mu\text{m}$ , is placed in a kick drum, and tensed under both uniform and non-uniform tension fields (described in detail in Section 4.4). After the tension is set up, four rectangular magnets of  $36 \text{ mm} \times 16 \text{ mm}$  are placed by pairs on each side of the membrane, to impose two zero displacement zones and to avoid introducing normal ( $z$ ) and tangential static deformations of the membrane. The magnets are held by a wood structure tied to the body of the drum, as seen in Fig. 3a.



(a) Structure configuration without the membrane.



(b) Vacuum measurement.

Fig. 3: Experimental setup for both landscape and modal measurements.

### 4.2. Modal measurement configuration

Most of the literature on modal analysis of plates or shells consider the light fluid assumption, disregarding the fluid loading on the structure. In the case of the membrane coupled to a cavity, the influence of the surrounding air cannot be neglected. Chaigne [27] shows that for circular membranes coupled with a cavity, the axisymmetric modes are the most affected by the added stiffness of the cavity increasing the natural frequencies. The air loading can also act as an added mass and the natural frequency is lowered this time. To avoid this effect, modal measurements will be carried inside a vacuum chamber. The vacuum conditions are at approximately  $1/300$  the atmospheric pressure (A.P.) ( $\sim 3 \text{ hPa}$ ), which is the practical limit of our vacuum chamber.

Modal analysis is performed using an impact excitation through an automatic impact hammer carrying a force sensor. The hammer is driven by an Arduino controller employed to set the impact period and the impact time length. The velocity field of the membrane is measured on 465 points employing a Polytec PSV-400 scanning laser vibrometer triggered on the impact force. The frequency response of the displacement over the force (receptance) is then derived on the frequency range  $[0.2 - 250] \text{ Hz}$  with a resolution of  $0.2 \text{ Hz}$ .

Localized modes prediction in a membrane with non-uniform tension from the quasi-static measurement of its localization landscape.

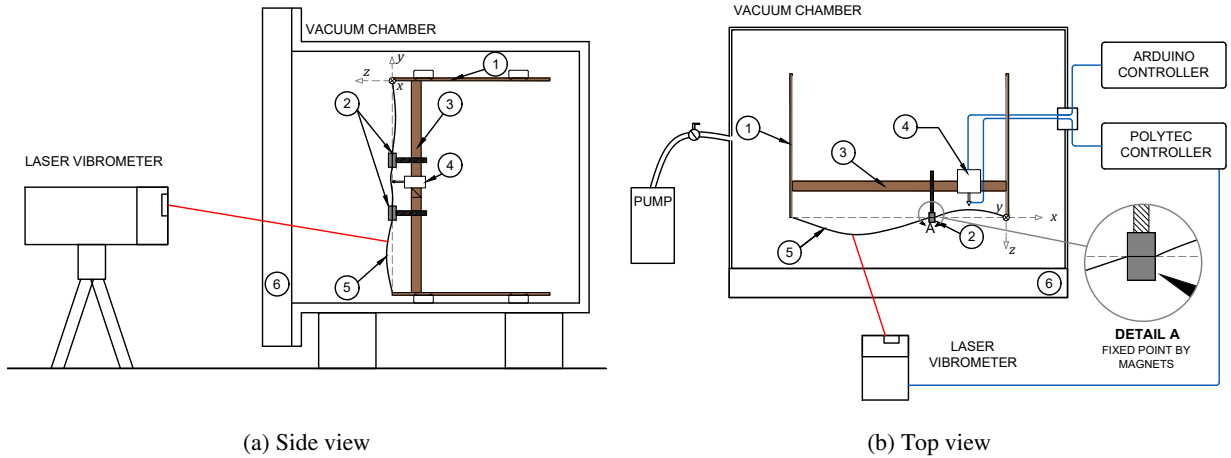


**Fig. 4:** Modal measurement set-up: 1. kick-drum cavity, 2. magnets used to create null displacement boundary conditions, 3. support structure, 4. automatic hammer (solenoid and force sensor), 5. membrane, 6. plexiglass door.

#### 4.2.1. Vacuum conditions

It is well known that as the tension on a membrane increases, the coupling between the air cavity and the membrane becomes weaker. Multiple values of tension were tested to derive the optimal experimental conditions for both landscape and modal measurements. Fig. 5 shows the evolution of the frequency of the first mode as function of the pressure inside the cavity, for two dissimilar tension conditions around  $700 \text{ N}\cdot\text{m}^{-1}$  and  $2200 \text{ N}\cdot\text{m}^{-1}$  (estimated with Eq. (13)). It is shown that the frequency of the first mode converges faster for the higher tension case. In fact, the normalized frequency (by the value obtained at 1/300 A.P.) exceeds 0.95 above 1/10 A.P. against 1/100 A.P. for the less tensed membrane. In the following, measurements will be then performed around a pressure of 1/300 A.P. to minimize the effect of air loading as much as possible.

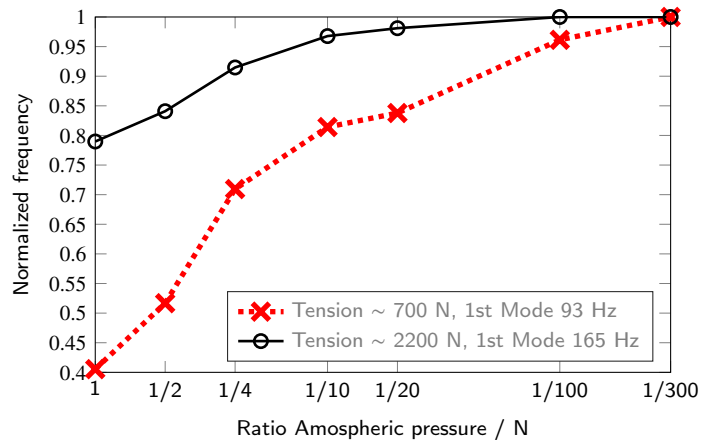


**Fig. 5:** Influence of the atmospheric pressure on the evolution of the first mode frequency at different ratios. A 'low' and 'high' uniform tension values are presented here.

#### 4.3. Landscape measurement configuration

The landscape function is determined from a static deformation measurement. To this aim, several techniques can be implemented: holographic interferometry [30], electronic speckle pattern interferometry [31] or digital speckle pattern interferometry [32]. However, these techniques require specialized equipment. The approach used in this work is based on a measure of the quasi-static deformation, allowing the use of a dynamic sensor. The frequency of excitation

must be much smaller than the first vibration mode, so that the quasi-static regime approximates the static regime (as seen in Eq. (8)), and much smaller than the first cavity mode to guarantee a uniform pressure load. The first cavity mode is found around 120 Hz at normal atmospheric pressure ( $\sim 1000$  hPa) and the first mode of the membrane is expected to be above 100 Hz. A suitable excitation frequency is chosen at 12 Hz. The kick drum cavity is sealed at its back face with 1-inch thick plywood where a 6-inch diameter loudspeaker is installed. The air cavity will act as an intermediate media to impose a uniform pressure on the membrane, that is monitored with a microphone (referenced by 4 on Fig. 6). The first pair of magnets are placed inside of the cavity in the same plane of the membrane, and the second pair of magnets will block the membrane on the other side without adding any static force. The membrane displacement under the harmonic acoustic excitation is then measured on 1013 points, averaging on 16 cycles, through a Polytech PSV-400 scanning laser vibrometer, configured in fast-scan mode.

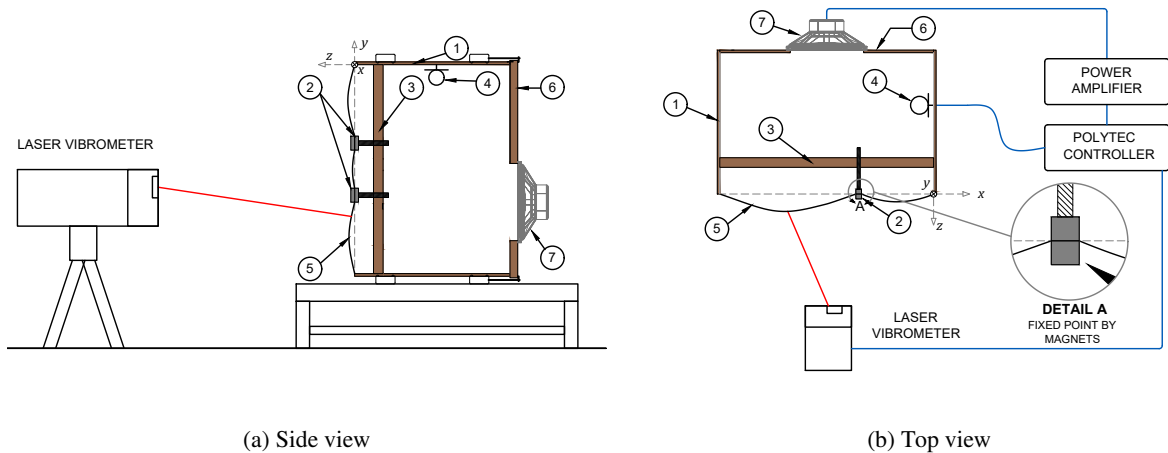


**Fig. 6:** Landscape measurement configuration: 1. bass-drum cavity, 2. magnets used to create null displacement boundary conditions, 3. support structure, 4. microphone, 5. membrane, 6. back enclosure, 7. loudspeaker.

## 4.4. Setting the membrane's tension

### 4.4.1. Uniform tension

This section describes the method to set the membrane tension. Achieving a perfect uniform tension is a challenging task. Most musicians, for example, tune their instruments, even if the tension is not perfectly uniform, by adjusting the frequency pitch when kicking specific parts of the membrane [33], or using commercially available tuners such as the Drum dial, which measures the deformation caused by its own load on the membrane. Chaigne [27] exposes the process to calculate the tension using the deflection caused by a small section load and gravity, but this method requires a static deformation measurement. The low sensitivity of the torque-meter wrench and the manufacturing uncertainties do not allow the use of imposed force on the tuning rods to guarantee a uniform tension.

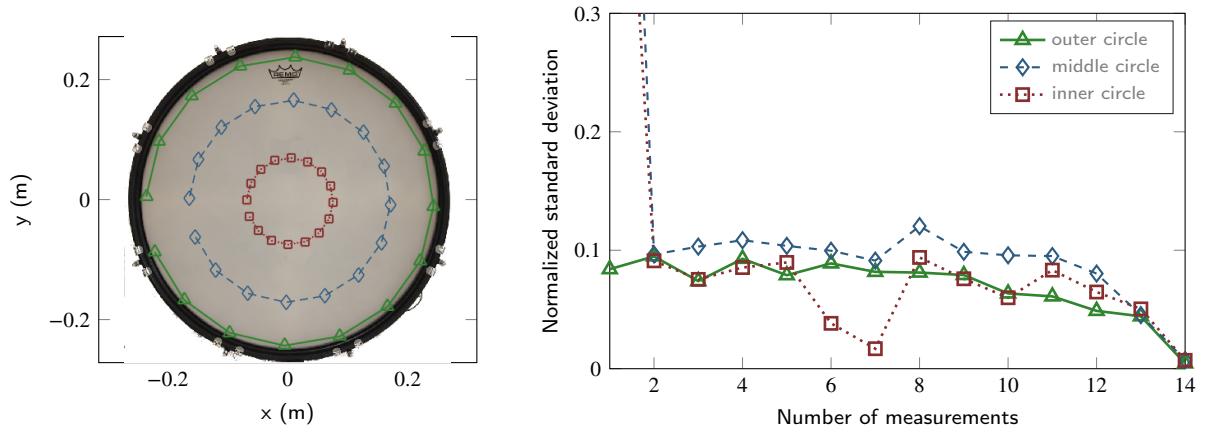
Our approach is to use the quasi-static deformation of the simple circular membrane under uniform load, as described in the previous section, to reach a circularly symmetric deformation, and hence, a uniform tension. Several measurement steps are shown in Fig. 8a to illustrate the method. Between each step, the tension is adjusted by acting on the tension rods surrounding the kick drum, accordingly to the displacement map. The displacement is measured around seven concentric circles on the membrane; the position of three of them are shown in Fig. 7a.

After 14 tuning steps, the most uniform tension state is considered achieved. As shown in Fig. 7b, the standard deviation of displacement approaches zero on 3 of the 7 concentric circles used to tune the membrane. The main disadvantage of this methodology is that it will be very hard to target a specific tension value due to the nature of the iterative process, as exposed in Section 4.4. This method has also been used to monitor the non-uniform configuration described below.

### 4.4.2. Non-uniform tension

To get the non-uniform tension configuration (see Fig. 8b), the uniform tension state is first achieved. Then, the tension rods are relaxed on the left side to create a smooth variation of the tension around the surface. This relaxation

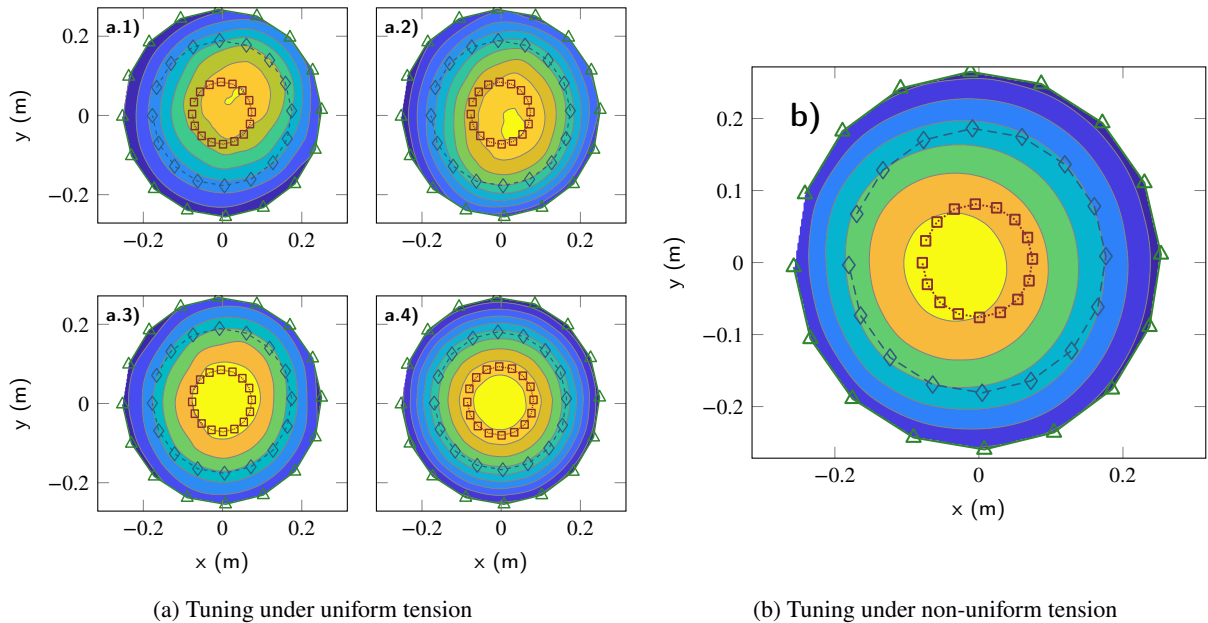
Localized modes prediction in a membrane with non-uniform tension from the quasi-static measurement of its localization landscape.



(a) 3 of 7 concentric circles used to tune up the membrane.

(b) Standard deviation of the displacement around 16 concentric points in 3 different concentric circles.

**Fig. 7:** Tuning up the membrane based on the measurement of the displacement in the concentric circles and the standard deviation.



(a) Tuning under uniform tension

(b) Tuning under non-uniform tension

**Fig. 8:** a) Displacement field during the process of tuning the membrane's tension by seeking an homogeneous deformation of the membrane, from the initial state: a.1), to the final state: a.4). The 3 concentric circles show the measurement points. b) Displacement field of the membrane under non-uniform tension field.

process is done carefully to maintain the linearity of the membrane behaviour and to avoid the presence of wrinkles along the membrane's surface.

## 5. Results

### 5.1. Uniform tension case

Once the iterative process end and the membrane is tensed under uniform tension, the tension is estimated with Eq. (13) at  $1890 \text{ N.m}^{-1}$ . Then, the magnets are placed as shown in Section 4.3. The cavity is airtightly sealed and an harmonic excitation at 12 Hz is driven by the loudspeaker. The acoustic pressure inside the cavity is 10.4 Pa.

Localized modes prediction in a membrane with non-uniform tension from the quasi-static measurement of its localization landscape.

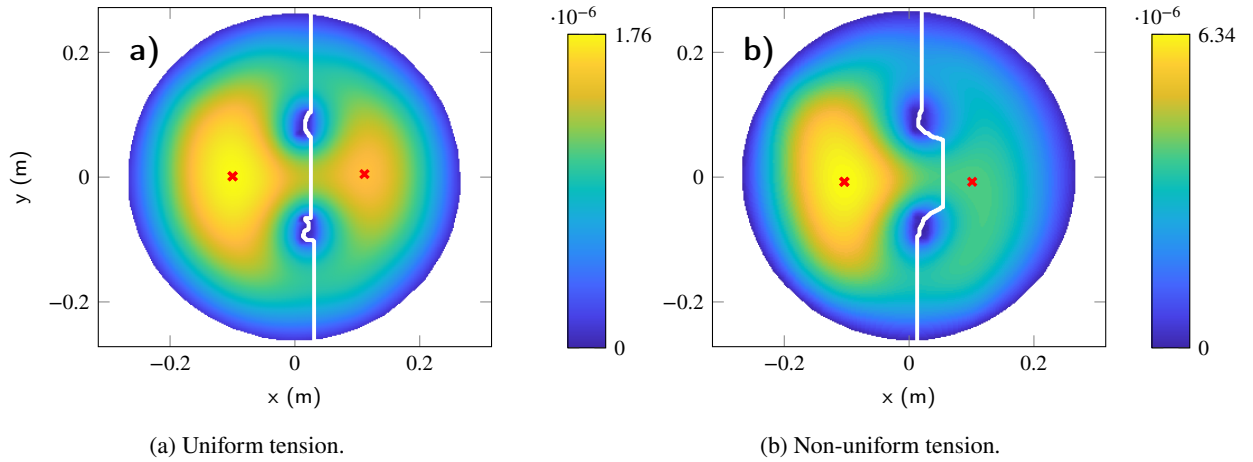


Fig. 9: Landscape measurements,  $u$  ( $s^2$ ).

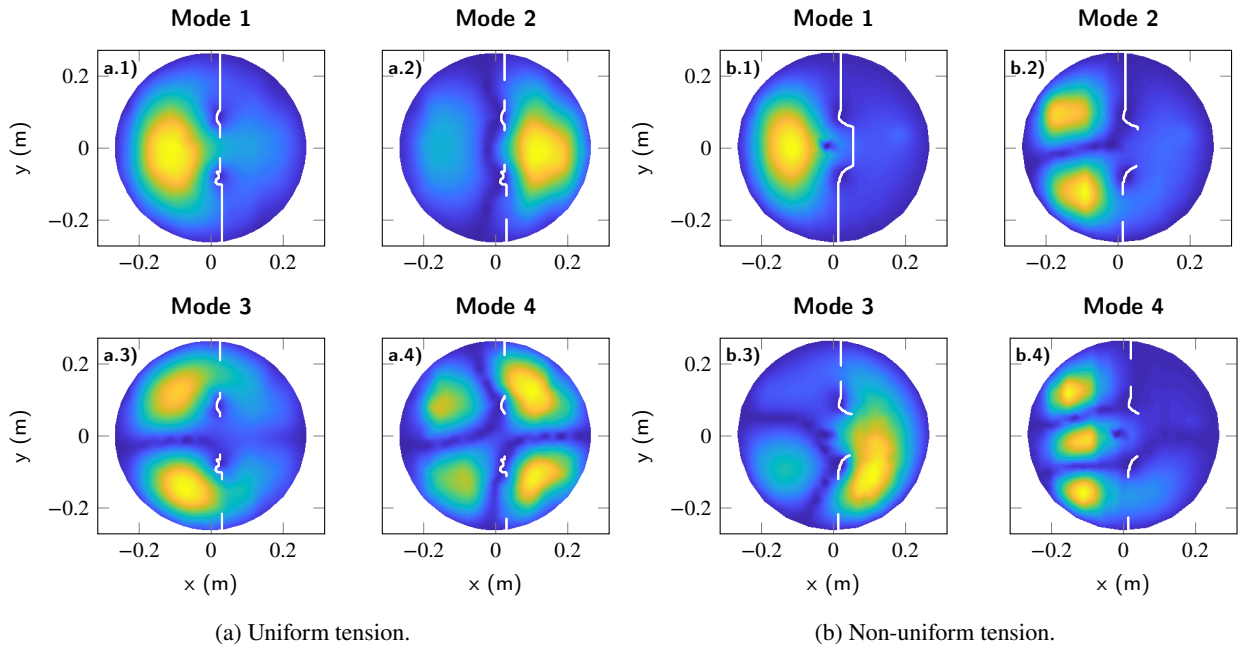


Fig. 10: Modal measurements.

Table 2

Measurements: Membrane under two different tension configurations. [1] Computed in PLM Siemens [2] Calculated with Eq. (17)

	Uniform Tension			Non-uniform Tension		
	Measured <sup>1</sup> (Hz)	Landscape <sup>2</sup> (Hz)	diff. %	Measured <sup>1</sup> (Hz)	Landscape <sup>2</sup> (Hz)	diff. %
<b>Mode 1</b>	149.74	152.54	+1.87	80.65	80.45	-0.24
<b>Mode 2</b>	174.67	168.43	-3.57	96.87	-	-
<b>Mode 3</b>	195.67	-	-	106.25	102.74	-3.30
<b>Mode 4</b>	223.92	-	-	116.56	-	-

The landscape measurement is presented in Fig. 9. Two main lobes arise over the landscape, indicating the presence of two localized modes in these regions. The white line corresponds to the network of valley lines and it is calculated by the watershed algorithm. This valley line separates our structure into 2 regions. The peak values in each region give an approximation of the localized modes frequencies according to Eq. (15) and are presented in Table 2.

Alternatively, from the modal measurement, the four first modes are presented in Fig. 10a. The projection of the effective valley network onto the modes is frequency-dependent and is calculated with Eq. (16). As we can see, when frequency increases, the valley lines tend to open allowing the modes to extend. The valleys must not be mistaken with the modal lines, but as a reference that will guarantee the geographical limits of localized modes and the strength of their confinement.

The estimation of localized modes frequencies, using Eq. (16), shows a difference between them and the measurement of less than 2% and 4% for the first and second mode respectively (refer to Table 2). When comparing the simulations and measurements in the uniform case, the simulations do not match exactly the experiment, showing a small difference of 3% on frequencies. This can be explained by the fact that it is quite difficult to ensure a perfectly uniform tension, as well as the uncertainty on the exact position of the magnets. The landscape function provides a pretty good estimation of the frequencies of the localized modes, with a difference of the same order as the one obtained by the simulation. Note that this estimation does not require knowledge of the tension value.

## 5.2. Non-uniform tension case

The tension field is relaxed on the left side of the membrane (see Fig. 8b) allowing a greater displacement on that side. The order of the modes is modified as in the preliminary numerical test. Interestingly, not only the fourth mode changed but also the second mode. The second mode is now localized on the same side as the first mode, and the third mode of the membrane corresponds to the localized mode on the right side of the membrane. Despite this change, the landscape theory identifies correctly the first localized mode in each region. The frequencies of both localized modes again are well estimated by the landscape function, a difference below 4% is found in this case, and even of less than 0.5% for the first mode, showing the predictive ability of the landscape function regardless of the tension field.

The choice of a linear variation of the tension field without shear is not enough to characterize the behaviour of the complex tension field present in this experiment. Trying to recreate such a non-uniform tension field would probably require a more complex field involving the presence of shear.

## 6. Conclusion

In conclusion, we demonstrate that the landscape function can be simply computed from the quasi-static deformation of a complex membrane. The quasi-static measurement of the landscape function allows determining the frequencies of the localized modes in the membrane, regardless of the homogeneity of the tension field (uniform or non-uniform) or its strength (lower tension or higher tension).

For uniform and non-uniform tension, a comparison between modal analysis and landscape of localization theory provides a good agreement. Localized modes are well-identified in both cases by the landscape computation with a difference of less than 5%.

The landscape function is a practical tool to characterize localized modes in complex membrane structures and by extension in other types of structures. Particularly in the case of a membrane, the direct measurement of the landscape function allows us to ignore the shape and values of the tension field, and still recover precisely the modal frequencies.

Even in complex cases, such as a membrane under non-uniform tension, the landscape function indicates the first localized modes in each sub-region, constrained geographically by the valley lines network.

## References

- [1] G. Lefebvre, M. Dubois, R. Beauvais, Y. Achaoui, Ros K. Ing, S. Guenneau, and P. Sebbah. Experiments on maxwell's fish-eye dynamics in elastic plates. *Appl. Phys. Lett.*, 106(2):024101, 2015. doi: 10.1063/1.4905730.
- [2] J. W. Segura, D. E. Patterson, A. J. LeRoy, G. R. May, and L. H. Smith. Percutaneous Lithotripsy. *J. Urology*, 130(6):1051–1054, December 1983. doi: 10.1016/S0022-5347(17)51678-X.
- [3] M. Fink. Time reversal of ultrasonic fields. i. basic principles. *IEEE Trans. Ultrason. Ferroelectr. Freq. Control*, 39(5):555–566, 1992. doi: 10.1109/58.156174.
- [4] A. L. Yarin, M. Pfaffenlehner, and C. Tropea. On the acoustic levitation of droplets. *J. Fluid Mech.*, 356:65–91, February 1998. ISSN 1469-7645, 0022-1120. doi: 10.1017/S0022112097007829.

Localized modes prediction in a membrane with non-uniform tension from the quasi-static measurement of its localization landscape.

- [5] M. Baudoin, J.-C. Gerbedoen, A. Riaud, O. B. Matar, N. Smagin, and J.-L. Thomas. Folding a focalized acoustical vortex on a flat holographic transducer: Miniaturized selective acoustical tweezers. *Sci. Adv.*, 5(4):eaav1967, April 2019. ISSN 2375-2548. doi: 10.1126/sciadv.aav1967.
- [6] J. Shi, D. Ahmed, X. Mao, Sz-Chin Steven Lin, A. Lawit, and T. Jun Huang. Acoustic tweezers: patterning cells and microparticles using standing surface acoustic waves (SSAW). *Lab Chip*, 9(20):2890–2895, 2009. doi: 10.1039/B910595F.
- [7] M. Yoneyama, J.-i. Fujimoto, Y. Kawamo, and S. Sasabe. The audio spotlight: An application of nonlinear interaction of sound waves to a new type of loudspeaker design. *J. Acoust. Soc. Am.*, 73(5):1532–1536, May 1983. ISSN 0001-4966. doi: 10.1121/1.389414.
- [8] P. W. Anderson. Absence of diffusion in certain random lattices. *Phys. Rev.*, 109:1492–1505, Mar 1958. doi: 10.1103/PhysRev.109.1492.
- [9] S. He and J. D. Maynard. Detailed measurements of inelastic scattering in anderson localization. *Phys. Rev. Lett.*, 57:3171–3174, Dec 1986. doi: 10.1103/PhysRevLett.57.3171.
- [10] C. Even, S. Russ, V Repain, P. Pieranski, and B. Sapoval. Localizations in fractal drums: An experimental study. *Phys. Rev. Lett.*, 83:726–729, Jul 1999. doi: 10.1103/PhysRevLett.83.726.
- [11] E. Chulkin, A. Zhernov, and T. Kulagina. Weak localization of low-frequency sound in a quasi-one-dimensional crystal. *Low Temp. Phys.*, 26:128–129, 02 2000. doi: 10.1063/1.593876.
- [12] M Filoche and S. Mayboroda. Strong Localization Induced by One Clamped Point in Thin Plate Vibrations. *Phys. Rev. Lett.*, 103(25):254301, December 2009. ISSN 0031-9007, 1079-7114. doi: 10.1103/PhysRevLett.103.254301.
- [13] M. Filoche and S. Mayboroda. Universal mechanism for Anderson and weak localization. *Proc. Natl. Acad. Sci. U.S.A.*, 109(37):14761–14766, September 2012. ISSN 0027-8424, 1091-6490. doi: 10.1073/pnas.1120432109.
- [14] G. Lefebvre, A. Gondel, M. Dubois, M. Atlan, F. Feppon, A. Labbé, C. Gillot, A. Garelli, M. Ernoult, S. Mayboroda, M. Filoche, and P. Sebbah. One Single Static Measurement Predicts Wave Localization in Complex Structures. *Phys. Rev. Lett.*, 117(7):074301, August 2016. ISSN 0031-9007, 1079-7114. doi: 10.1103/PhysRevLett.117.074301.
- [15] F. Fahy and P. Gardonio. *Sound and Structural Vibration*. Academic Press, Oxford, second edition edition, 2007.
- [16] M. P. Norton and D. G. Karczub. *Fundamentals of Noise and Vibration Analysis for Engineers*. Cambridge University Press, 2 edition, 2003. doi: 10.1017/CBO9781139163927.
- [17] C. Lesueur. *Rayonnement acoustique des structures: vibroacoustique, interactions fluide-structure [Acoustic radiation of structures: vibroacoustics, fluid-structure interactions]*. Collection de la Direction des études et recherches d’Electricité de France. Eyrolles, 1988. ISBN 9782212016130.
- [18] W Soedel. *Vibration and Sound*. Marcel Dekker Inc., New York, third edition edition, 2004.
- [19] P. M. Morse and K. U. Ingard. *Theoretical acoustics*. McGraw-Hill, New York, 1968.
- [20] T. D. Rossing. Acoustics of Drums. *Phys. Today*, 45(3):40, January 2008. ISSN 0031-9228. doi: 10.1063/1.881333.
- [21] R. Worland. Drum tuning: an experimental analysis of membrane modes under non-uniform tension. *Proc. Meet. Acoust.*, 5(1):035001, November 2008. doi: 10.1121/1.3138888.
- [22] R. Worland. Normal modes of a musical drumhead under non-uniform tension. *J. Acoust. Soc. Am.*, 127(1):525–533, January 2010. ISSN 0001-4966. doi: 10.1121/1.3268605.
- [23] R. S. Christian, R. E. Davis, A. Tubis, C. A. Anderson, R. I. Mills, and T. D. Rossing. Effects of air loading on timpani membrane vibrations. *J. Acoust. Soc. Am.*, 76(5):1336–1345, November 1984. ISSN 0001-4966. doi: 10.1121/1.391449.
- [24] J. Calder. New research on low-frequency membrane absorbers. *Proc. Meet. Acous.*, 33(1):015001, May 2018. doi: 10.1121/2.0000816.
- [25] H. Wagner. Ebene blechwandträger mit sehr dünnem stahlblech [flat sheet metal girders with very thin sheet web]. *Z. Flugtechnik und Motorluftschiffahrt*, 20(8-12), 1929.
- [26] K. Kondo. The geometry of the perfect tension field. *J. Soc. Appl. Mech. Jpn.*, 3:36–39, 85–89, 1950.
- [27] A. Chaigne. *Acoustique des instruments de musique [Acoustics of Musical Instruments]*. Belin, 2008.
- [28] R. Mahmoudi and M. Akil. Analyses of the Watershed Transform. *Int. J. Imag. Process.*, 5(5):521–541, 2011. URL <https://hal-upec-upem.archives-ouvertes.fr/hal-01294109>.
- [29] F. Hecht. New development in freefem++. *J. Numer. Math.*, 20(3-4):251–265, 2012. ISSN 1570-2820. URL <https://freefem.org/>.
- [30] J. Frejlich and P. M. Garcia. Advances in real-time holographic interferometry for the measurement of vibrations and deformations. *Opt. Lasers Eng.*, 32(6):515–527, December 1999. ISSN 0143-8166. doi: 10.1016/S0143-8166(99)00073-1.
- [31] L. Yang, X. Xie, L. Zhu, S. Wu, and Y. Wang. Review of electronic speckle pattern interferometry (ESPI) for three dimensional displacement measurement. *Chin. J. Mech. Eng.*, 27(1):1–13, January 2014. ISSN 2192-8258. doi: 10.3901/CJME.2014.01.001.
- [32] R. Kumar, I. P. Singh, and C. Shakher. Measurement of out-of-plane static and dynamic deformations by processing digital speckle pattern interferometry fringes using wavelet transform. *Opt. Lasers Eng.*, 41(1):81–93, January 2004. ISSN 0143-8166. doi: 10.1016/S0143-8166(02)00118-5.
- [33] J. S. Johnson. Drum Tuning Bible, July . URL <https://bit.ly/2MZUM9J>. (Last accessed: 19 September 2020, [Online]).